ELSEVIER

Journal of the Mechanics and Physics of Solids
52 (2004) 1–26

JOURNAL OF THE
MECHANICS AND
PHYSICS OF SOLIDS

www.elsevier.com/locate/jmps

The influence of mechanical deformation on the electrical properties of single wall carbon nanotubes

B. Liu, H. Jiang, H.T. Johnson*, Y. Huang

Department of Mechanical and Industrial Engineering, University of Illinois, Urbana, IL 61801, USA

Received 2 November 2002; accepted 1 July 2003

Abstract

Recent experimental studies and atomistic simulations have shown that carbon nanotubes (CNTs) display strong interplay between the mechanical deformation and electrical properties. We have developed a simple and accurate method to determine atom positions in a uniformly deformed CNT via a continuum analysis based on the interatomic potential. A shift vector is introduced to ensure the equilibrium of atoms. Such an approach, involving only three variables for the entire CNT, agrees very well with the molecular mechanics calculations. We then study the effect of mechanical deformation on the band gap change of single wall CNTs under tension, torsion, and combined tension/torsion via the k-space tight-binding method. Prior studies without this shift vector lead to significant overestimation of the band gap change. It is established that the conducting CNTs may easily become semi-conducting ones subject to mechanical deformation, but the semi-conducting CNTs never become conducting ones upon deformation.

Keywords: Carbon nanotube; Electromechanical processes; Continuum analysis; Tight-binding; Semiconductor material

1. Introduction

Carbon nanotubes (CNTs) have received significant attention since their first discovery a decade ago (Iijima, 1991). CNTs display superior mechanical properties, such as ultra high elastic moduli, strength, and low mass density, and have potential applications in composite materials and other mechanical systems. CNTs have unique electrical properties, and can serve as candidates for nano-electronic devices such as

* Corresponding author.
E-mail address: htj@uiuc.edu (H.T. Johnson).

0022-5096/$ - see front matter
doi:10.1016/S0022-5096(03)00112-1

nanoscale field-effect transistors (Collins et al., 2001; Rosenblatt et al., 2002). CNTs also display unique interplay between the electrical properties and mechanical deformation (Bezryadin et al., 1998; Paulson et al., 1999; Gaal et al., 2000; Tombler et al., 2000; Liu et al., 2001b). For example, Tombler et al. (2000) investigated the change of electrical conductance for a single wall CNT (i.e., a single layer of carbon atoms) due to bending. The samples of individual single wall CNTs were prepared to bridge metal electrodes on SiO_2/Si substrates. Part of the CNT length was suspended over trenches fabricated on the SiO_2 surface, and the suspended CNT was bent mechanically by the tip of an atomic force microscope. The change in the electrical conductance was measured simultaneously upon mechanical deformation. Tombler et al. (2000) found that the deformation of a CNT is completely reversible even under large deformation (for strain more than a few percent). Moreover, the electrical conductance may change by two orders of magnitude upon mechanical deformation. This strong coupling between the electrical properties and mechanical deformation has many potential applications, such as nanoscale sensors and nano-electro-mechanical systems (NEMS). In another experiment, however, Paulson et al. (1999) measured the electrical resistance of a multiwall CNT during mechanical deformation, and they did not observe change of electrical resistance associated with deformation. These experiments have motivated extensive atomistic studies on the coupling between electrical property and mechanical deformation, such as the tight-binding calculations for CNTs under tension (Heyd et al., 1997; Yang et al., 1999; Nardelli et al., 2000), torsion (Rochefort et al., 1999; Yang et al., 1999), bending (Nardelli, 1999; Nardelli and Bernholc, 1999; Rochefort et al., 1999; Liu et al., 2000, 2001a; Nardelli et al., 2000; Tombler et al., 2000), as well as first-principle calculations on CNTs under bending (Maiti, 2000; Mazzoni and Chacham 2000a) and flattening (Mazzoni and Chacham, 2000b; Peng and Cho, 2002).

The tight-binding calculations of Liu et al. (2000) and Tombler et al. (2000) suggested that an armchair single wall CNT subject to localized bending (e.g., due to pushing by the tip of an atomic force microscope) may experience significant atomic structure change from sp^2 to sp^3. This change of atomic structure may cause significant reduction in the electrical conductance of the single wall CNT, as observed in Tombler et al.'s (2000) experiment. Rochefort et al. (1999) and Mazzoni and Chacham (2000a) used the tight-binding method and first-principle calculations respectively to investigate a single wall CNT under global (rather than localized) bending, and also found significant electrical property change during bending. They observed the local kinking of single wall CNTs under very large bending curvatures, and such localized deformation also leads to the change of atomic structure from sp^2 to sp^3. However, Nardelli (1999), Nardelli and Bernholc (1999), and Nardelli et al. (2000) did not report any localized kinking of single wall CNTs in their tight-binding calculations for relatively small bending curvatures. They did not observe the change of atomic structure from sp^2 to sp^3.

There are tight-binding calculations of CNTs under tension. A schematic diagram of a CNT is shown in Fig. 1a. Yang et al. (1999) investigated the band gap change for a single wall CNT subject to *uniaxial strain* along the axial direction Z of the CNT (i.e., $\varepsilon_{ZZ} \neq 0$ and other $\varepsilon_{ij} = 0$). In order to illustrate Yang et al.'s (1999)

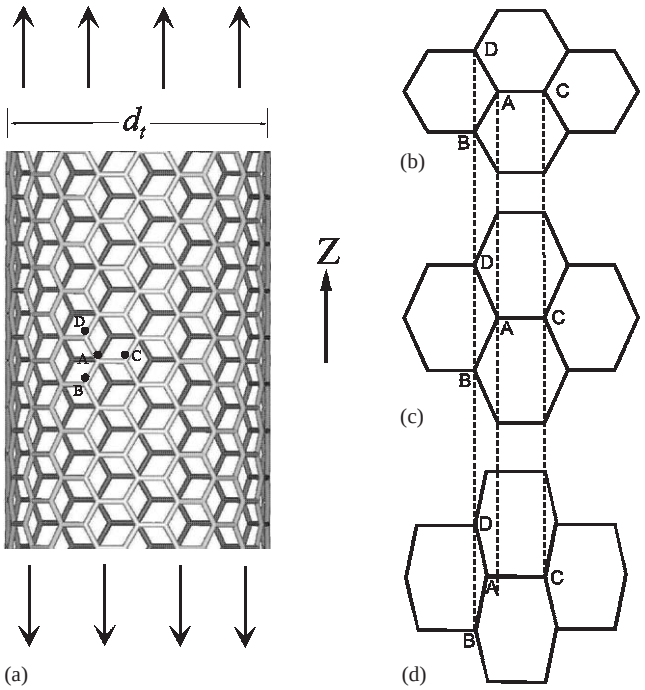

Fig. 1. Schematic illustrations of a carbon nanotube (CNT) under tension. (a) A schematic diagram of CNT with the diameter d_t, a representative atom A and its three nearest-neighbor atoms B, C and D. (b) Positions of atoms A, B, C and D prior to deformation. (c) Positions of atoms A, B, C and D based on an assumed simple deformation pattern for a CNT subject to uniaxial strain ($\varepsilon_{ZZ} \neq 0$ and other $\varepsilon_{ij} = 0$); such a simple deformation pattern does not satisfy the equilibrium condition. (d) The actual, relaxed positions of atoms A, B, C and D on a CNT subject to uniaxial strain; the equilibrium of atoms is ensured.

approach of determining the atom positions, Fig. 1b presents a two-dimensional diagram of the undeformed, hexagonal atomic structure, which is identical to a graphite plane. Fig. 1c shows the deformed atomic structure following the assumed simple, uniform deformation pattern $\varepsilon_{ZZ} \neq 0$ and other $\varepsilon_{ij} = 0$ for all atoms. The axial coordinate Z of each atom becomes $(1 + \varepsilon_{ZZ})Z$, while the coordinates in the directions normal to Z remain unchanged (since other $\varepsilon_{ij} = 0$). This is illustrated by the dashed lines in Figs. 1b and c. Heyd et al. (1997) made a similar assumption to determine the atomic positions in the CNT subject to uniaxial tension ($\boldsymbol{\sigma}_{ZZ} \neq 0$, other $\boldsymbol{\sigma}_{ij} = 0$), and they used the linear elastic constant of graphite to estimate the strains. Once the atomic positions are determined, Heyd et al. (1997) and Yang et al. (1999) calculated the band gap of the single wall CNT by the tight-binding method. They both found that the armchair CNTs remain conductive during tension, but the electrical conductance of zigzag CNTs is much more complex. Here armchair and zigzag CNTs refer to different orientations of carbon bonds, which is discussed in detail in Section 2. Yang et al. (1999) also determined the atomic positions in CNTs under tension by the molecular mechanics energy minimization based on Brenner's (1990) interatomic potential,

and confirmed their conclusion on the coupling between mechanical deformation and electrical property change.

The same methods were adopted by Yang et al. (1999) to study CNTs under torsion. Contrary to tension, armchair CNTs under torsion exhibit significant change in the electrically conducting behavior. Rochefort et al. (1999) also reached the same conclusion using a molecular mechanics energy minimization scheme for atomic positions and the extended Huckel method for electrical properties.

One critical step in the above atomistic studies of the electrical property change due to mechanical deformation is the determination of atom positions on the deformed CNT. The molecular mechanics energy minimization (Rochefort et al., 1999; Yang et al., 1999) based on Brenner's (1990) interatomic potential inevitably involves many carbon atoms and requires computational effort. The simple, uniform deformation pattern assumed for all atoms (Heyd et al., 1997; Yang et al., 1999) is much simpler, but it may not be accurate since the equilibrium of atoms cannot be ensured, which is illustrated in the following. For a CNT subject to uniaxial strain ($\varepsilon_{ZZ} \neq 0$ and other $\varepsilon_{ij} = 0$), the length AC in Fig. 1c after deformation remains the same as AC in Fig. 1b prior to deformation, since AC is normal to the loading direction Z. For the same reason, the projection of AB normal to the Z direction also remains unchanged, but AB becomes longer in the stretch direction Z (Fig. 1c). The stretching in AB (as well as in AD) leads to a net force on the atom A. Therefore, the assumed simple deformation pattern cannot ensure equilibrium of atom A, and is not correct. In fact, the position of atom A needs to be "relaxed" after deformation in order to find its equilibrium position (Fig. 1d). The inaccuracy in the atom position will lead to errors in the electrical property calculation.

The purpose of the present study is to develop a rather simple but accurate method for the determination of atom positions and to apply this method to the study of tight-binding based electronic properties of a range of nanotubes under general uniform deformations. Taking advantage of the periodic atomic structure of CNTs, we find that only three variables are needed to characterize the positions of all atoms in a uniformly deformed CNT, and these three variables can be determined from the equilibrium equations. Therefore, the computational effort to determine atom positions is significantly reduced. Fig. 1d shows a schematic diagram of our approach to relax atom A searching for its equilibrium position. Section 2 provides the details of our method, which modifies Heyd et al.'s (1997), and Yang et al.'s (1999) method to ensure the equilibrium of atoms in the calculation of the atom positions after deformation. We then adopt the k-space tight-binding method to calculate the electrical property change for a single wall CNT subject to tension, torsion and combined tension/torsion in Section 3. The band gap versus deformation is shown in Section 4, and results are also compared with available atomistic studies. The effect of finite temperature is discussed in Section 5.

2. Atom positions on a carbon nanotube

Brenner's (1990) empirical interatomic potential for carbon has been widely used in the study of CNTs, and is summarized below.

2.1. The interatomic potential for carbon

Brenner (1990) established a multi-body interatomic potential for carbon as

$$V(r_{ij}) = V_R(r_{ij}) - B_{ij}V_A(r_{ij}), \tag{1}$$

where r_{ij} is the length between two atoms i and j, V_R and V_A are the repulsive and attractive pair terms given by

$$V_R(r) = \frac{D^{(e)}}{S-1}\,\mathrm{e}^{-\sqrt{2S}\beta(r-R^{(e)})}f_c(r), \quad V_A(r) = \frac{D^{(e)}}{S-1}\,\mathrm{e}^{-\sqrt{(2/S)}\beta(r-R^{(e)})}f_c(r), \tag{2}$$

where $D^{(e)} = 6.000$ eV, $S = 1.22$, $\beta = 21$ nm^{-1}, and $R^{(e)} = 0.1390$ nm. The function f_c in (2) is a smooth cut-off function given by

$$f_c(r) = \begin{cases} 1 & r < R^{(1)}, \\ \dfrac{1}{2}\left\{1 + \cos\left[\dfrac{\pi(r-R^{(1)})}{R^{(2)}-R^{(1)}}\right]\right\} & R^{(1)} < r < R^{(2)}, \\ 0 & r > R^{(2)}, \end{cases} \tag{3}$$

where the effective range of the cut-off function is defined by $R^{(1)} = 0.17$ nm and $R^{(2)} = 0.20$ nm. The term B_{ij} in (1) represents a multi-body coupling effect (i.e., the contribution from atoms other than i and j), and is given by

$$B_{ij} = \left[1 + \sum_{k(\neq i,j)} G(\theta_{ijk})f_c(r_{ik})\right]^{-1/2}, \tag{4}$$

where $k(\neq i,j)$ denotes the other carbon atoms, f_c is given in (3), θ_{ijk} is the angle between $i-j$ and $i-k$ bonds, and the function G is given by

$$G(\theta) = a_0\left[1 + \frac{c_0^2}{d_0^2} - \frac{c_0^2}{d_0^2 + (1+\cos\theta)^2}\right], \tag{5}$$

$a_0 = 0.00020813$, $c_0 = 330$ and $d_0 = 3.5$.

2.2. Atom positions on a carbon nanotube prior to deformation

Unlike a graphite sheet, the carbon bonds on a nanotube have different lengths because of the finite diameter d_t of the CNT. In order to characterize its periodic lattice structure, the CNT is mapped to a two-dimensional sheet of carbon atoms in Fig. 2a. This can be visualized by "cutting" the CNT along its axial direction and "unrolling" the CNT to a plane without stretching. A representative atom A in Fig. 2a and its three nearest-neighbor atoms B, C, and D are shown in Fig. 2b. Let $\boldsymbol{a}_1$ and $\boldsymbol{a}_2$ denote the base vectors $\vec{BC}$ and $\vec{DC}$ in Fig. 2b, respectively, and a_1 and a_2 the corresponding lengths. The lengths of BD, AB, and AC are denoted by a_3, a_4 and a_5, respectively. These five lengths completely determine all in-plane lengths and angles. For example, the angles $\varphi_1 = \angle CBD$ and $\varphi_2 = \angle CBA$ (Fig. 2b) are given in terms of

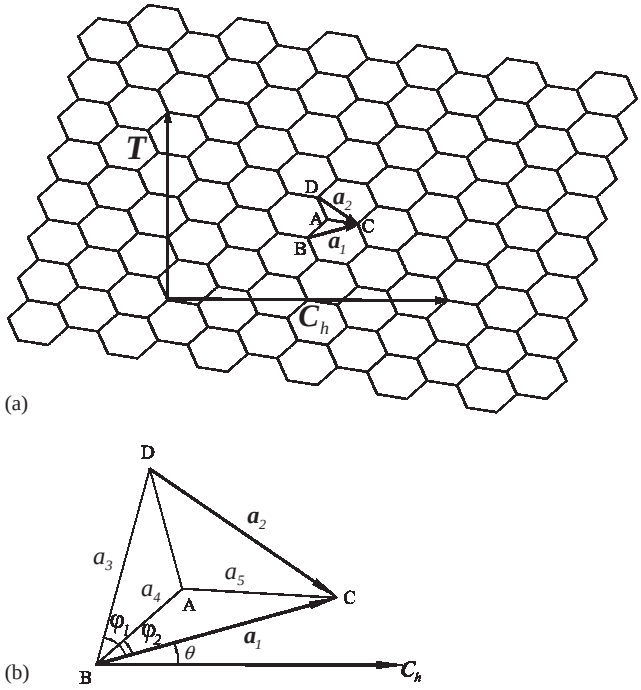

Fig. 2. A carbon nanotube (CNT) prior to deformation. (a) A planar, "unrolled" CNT; $\boldsymbol{C}_h$ and $\boldsymbol{T}$ are the chiral vector and translational vector of the CNT, respectively. (b) A representative atom A and its three nearest-neighbor atoms.

the above lengths a_i $(i = 1, 2, \ldots, 5)$ by

$$\varphi_1 = \cos^{-1}\frac{a_1^2 + a_3^2 - a_2^2}{2a_1a_3}, \quad \varphi_2 = \cos^{-1}\frac{a_1^2 + a_4^2 - a_5^2}{2a_1a_4}. \tag{6}$$

In order to characterize the bond lengths and angles of a CNT in the three-dimensional configuration, it is necessary to prescribe the diameter d_t as well as the angle θ between the base vector $\boldsymbol{a}_1 = \vec{BC}$ and the chiral vector $\boldsymbol{C}_h$ (Fig. 2b) in addition to the lengths a_i $(i = 1, 2, \ldots, 5)$, where the chiral vector $\boldsymbol{C}_h$ represents the circumferential direction of the CNT. Let (R, Θ, Z) denote the cylindrical coordinates of the CNT prior to deformation. The radial coordinates of all atoms are $R_A = R_B = R_C = R_D = d_t/2$. Without losing generality, we may take the polar angle and axial coordinate of atom B as zero, $\Theta_B = Z_B = 0$. The axial coordinates of atoms A, C, and D are given by (Fig. 2b)

$$Z_A = a_4 \sin(\varphi_2 + \theta), \quad Z_C = a_1 \sin\theta, \quad Z_D = a_3 \sin(\varphi_1 + \theta), \tag{7}$$

while their polar angles are given by (Fig. 2b)

$$\Theta_A = \frac{2a_4\cos(\varphi_2 + \theta)}{d_t}, \quad \Theta_C = \frac{2a_1\cos\theta}{d_t}, \quad \Theta_D = \frac{2a_3\cos(\varphi_1 + \theta)}{d_t}. \tag{8}$$

The bond length between two atoms X and Y $(X,Y=A,B,C,D)$ with coordinates $(d_t/2,\Theta_X,Z_X)$ and $(d_t/2,\Theta_Y,Z_Y)$ are then obtained in terms of a_i $(i=1,2,\ldots,5)$, d_t, and θ by

$$r_{XY}^{(0)}=\sqrt{\frac{d_t^2}{2}[1-\cos(\Theta_Y-\Theta_X)]+(Z_Y-Z_X)^2}. \tag{9}$$

The above bond length is different from the in-plane lengths a_i $(i=1,2,\ldots,5)$ since it is evaluated for the three-dimensional configuration of the CNT. It can be shown that, for $d_t\to\infty$, the bond length $r_{XY}^{(0)}$ approaches one of the in-plane length a_i $(i=1,2,\ldots,5)$, and becomes independent of θ. The energy stored in this bond XY is then obtained from Brenner's (1990) interatomic potential in (1) with the bond length calculated from (9).

The nanotube diameter d_t (Fig. 1a) and orientation θ (Fig. 2b) are related to the chirality (n,m) of the CNT. Following the standard notation for CNTs (e.g., Saito et al., 1998), the chiral vector $\boldsymbol{C}_h$ corresponds to the equator of the CNT (Fig. 2a) and can be expressed in terms of the base vectors $\boldsymbol{a}_1$ and $\boldsymbol{a}_2$ by

$$\boldsymbol{C}_h=n\boldsymbol{a}_1+m\boldsymbol{a}_2, \tag{10}$$

where n and m are integers. Without losing generality, $\boldsymbol{a}_1$ and $\boldsymbol{a}_2$ are chosen such that $n\geqslant|m|\geqslant 0$. The pair (n,m) is called the chirality of the CNT; $(n,0)$ and (n,n) are called zigzag and armchair CNTs, respectively, while $n>|m|>0$ is called a chiral CNT. For example, the chirality in Fig. 2a is (4,2). The circumference, diameter, and angle θ of the CNT are given in terms of lengths a_i $(i=1,2,\ldots,5)$ and chirality (n,m) by

$$|\boldsymbol{C}_h|=\sqrt{\boldsymbol{C}_h\cdot\boldsymbol{C}_h}=\sqrt{n^2a_1^2+m^2a_2^2+nm(a_1^2+a_2^2-a_3^2)}, \tag{11}$$

$$d_t=\frac{|\boldsymbol{C}_h|}{\pi}, \tag{12}$$

$$\theta=\cos^{-1}\frac{\boldsymbol{C}_h\cdot\boldsymbol{a}_1}{|\boldsymbol{C}_h|a_1}=\cos^{-1}\frac{na_1^2+\frac{m}{2}(a_1^2+a_2^2-a_3^2)}{|\boldsymbol{C}_h|a_1}. \tag{13}$$

Therefore, for a given chirality (n,m) of the CNT, the bond lengths in (9) as well as the energy $V(r_{AX})$ stored in bond AX $(X=B,C,D)$ are functions of $a_1,a_2,\ldots,a_5$. These lengths a_i $(i=1,2,\ldots,5)$ are different from the lattice constant of graphite, and are determined by minimizing the energy in the system. This is also equivalent to minimizing the energy per atom, i.e.,

$$\frac{\partial}{\partial a_i}[V(r_{AB})+V(r_{AC})+V(r_{AD})]=0,\quad i=1,2,\ldots,5. \tag{14}$$

Here only nearest-neighbor interaction is considered because Brenner's (1990) interatomic potential has a cutoff function that excludes interaction beyond the nearest-neighbor atoms. Once these lengths a_i $(i=1,2,\ldots,5)$ are determined, the atom positions on a CNT prior to deformation are known.

Table 1 shows the bond lengths and angles prior to deformation for two zigzag $[(10,0),(9,0)]$, one armchair $[(5,5)]$, and two chiral CNTs $[(9,6),(6,4)]$. The bond lengths and angles for a graphite sheet are also shown. It is important to note that,

Table 1
Bond lengths and angles of single wall carbon nanotubes prior to deformation

	Chirality	Conductor	Bond lengths (nm)			Bond angles (degree)		
	(n,m)		$r_{AB}^{(0)}$	$r_{AC}^{(0)}$	$r_{AD}^{(0)}$	$\angle BAC$	$\angle BAD$	$\angle CAD$
Graphite	$n+m\to\infty$	Yes	0.14507	0.14507	0.14507	120	120	120
Zigzag	(9,0)	Yes	0.14553	0.14553	0.14520	117.77	119.62	119.62
nanotubes	(10,0)	No	0.14544	0.14544	0.14518	118.20	119.69	119.69
Armchair nanotubes	(5,5)	Yes	0.14533	0.14568	0.14533	118.27	120.26	118.27
Chiral	(9,6)	Yes	0.14520	0.14553	0.14516	119.13	120.08	119.36
nanotubes	(6,4)	No	0.14538	0.14567	0.14528	118.04	120.21	118.59

even though bond lengths and angles are very close to those of a graphite sheet, these small differences may lead to changes in the band gap, as shown in Section 4. Some prior analyses using the lattice constant of graphite to approximate the lengths a_i $(i=1,2,\ldots,5)$ (e.g., Yang et al., 1999; Heyd et al., 1997) have not accounted for this important effect of unequal bond length due to the curvature of the CNT.

Since a CNT has periodicity along the axial direction Z, it is convenient to introduce a translational vector $\boldsymbol{T}$ (Saito et al., 1998), which is normal to $\boldsymbol{C}_h$ (i.e., parallel to Z) and its length is the period in Z direction. The number of hexagons within the area of $|\boldsymbol{C}_h\times\boldsymbol{T}|$ is given by $N=|\boldsymbol{C}_h\times\boldsymbol{T}|/|\boldsymbol{a}_1\times\boldsymbol{a}_2|$.

2.3. Atom positions on a carbon nanotube after deformation

2.3.1. A modified Cauchy–Born rule for carbon nanotubes

A single wall CNT subject to tension and/or torsion remains circular in cross-section. Following the same approach outlined in Section 2.2, we map the deformed CNT to a two-dimensional sheet of carbon atoms (similar to Fig. 2a for the undeformed CNT), i.e., to "unroll" the deformed CNT to a plane without stretching. However, the lengths between atoms, denoted by a_i $(i=1,2,\ldots,5)$ in Fig. 2b for the undeformed CNT, now depend on the imposed deformation, which is characterized by the Lagrangian strain components $E_{\Theta\Theta}$, E_{ZZ} and $E_{\Theta Z}(=E_{Z\Theta})$ in the cylindrical coordinates. In fact, it can be shown that this mapping of the deformed CNT to a plane is equivalent to the mapping of undeformed CNT (in Figs. 2a and b) followed by the in-plane deformation according to $E_{11}=E_{\Theta\Theta}$, $E_{22}=E_{ZZ}$, $E_{12}=E_{21}=E_{\Theta Z}(=E_{Z\Theta})$, where the subscript "1" represents the circumferential direction $\boldsymbol{C}_h$, and "2" is normal to $\boldsymbol{C}_h$ within the plane.

The deformation on the continuum level is characterized by the deformation gradient $\boldsymbol{F}=\partial\boldsymbol{x}/\partial\boldsymbol{X}$, where $\boldsymbol{x}$ and $\boldsymbol{X}$ denote the positions of a material point in the deformed and undeformed configurations, respectively, and $\boldsymbol{F}$ is related to the Lagrangian strain $\boldsymbol{E}$ by

$$\boldsymbol{E}=\frac{1}{2}(\boldsymbol{F}^{\mathrm{T}}\cdot\boldsymbol{F}-\boldsymbol{I}), \tag{15}$$

with $\boldsymbol{F}^{\mathrm{T}}$ being the transpose of $\boldsymbol{F}$ and $\boldsymbol{I}$ being the second order identity tensor.

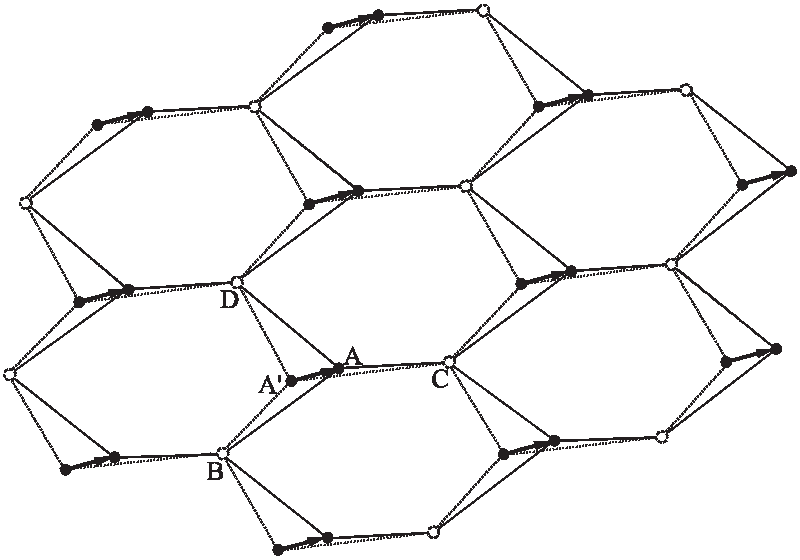

Fig. 3. The decomposition of a hexagonal lattice, "unrolled" from a deformed carbon nanotube, to two triangular sub-lattices. There is a shift vector $\boldsymbol{\zeta}$ between two sub-lattices to ensure the equilibrium of atoms. The solid and dotted lines denote the lattice structures with and without the shift vector $\boldsymbol{\zeta}$ respectively.

The Cauchy–Born rule (Born and Huang, 1954; Milstein, 1980) states that, for a centrosymmetric lattice structure subject to homogeneous deformation, the atoms move according to

$$\boldsymbol{r}_{ij} = \boldsymbol{F} \cdot \boldsymbol{r}_{ij}^{(0)}, \tag{16}$$

where $\boldsymbol{r}_{ij}^{(0)}$ and $\boldsymbol{r}_{ij}$ are vectors from atom i to atom j before and after the deformation, respectively. It is pointed out that (16) has accounted for the effect of finite deformation. The Cauchy–Born rule ensures the equilibrium of each atom in a centrosymmetric lattice structure because forces in each centrosymmetric pair of bonds are equal and opposite for arbitrarily imposed homogeneous deformation.

The Cauchy–Born rule (16), however, cannot be simply applied to CNTs since their lattice structure is not centrosymmetric, therefore cannot ensure the equilibrium of atoms. Weiner (1983), Johnson et al. (1999) and Tadmor et al. (1999) proposed modifications of the Cauchy–Born rule for bulk materials with non-centrosymmetric lattice structures, while Arroyo and Belytschko (2002) and Zhang et al. (2002a, b) modified the Cauchy–Born rule for CNTs. Zhang et al.'s (2002a, b) method is adopted in the present study.

As shown in Fig. 3, the hexagonal lattice "unrolled" from a deformed CNT can be decomposed to two triangular sub-lattices, marked by open circles and solid circles, respectively. Each sub-lattice possesses centrosymmetry such that each pair of atoms within the same sub-lattice moves according to the Cauchy–Born rule (16), but two atoms from different sub-lattices do not follow the Cauchy–Born rule. The dotted lines

in Fig. 3 represent the lattice structure if all atoms (from both sub-lattices) were to follow the Cauchy–Born rule, as illustrated by a representative atom A' from one (solid circle) sub-lattice, and its three nearest-neighbor atoms B, C, and D in the other (open circle) sub-lattice. As discussed earlier, such a lattice structure cannot ensure the equilibrium of atom A'. In order to overcome this drawback, we introduce a shift vector $\boldsymbol{\zeta}$ between two sub-lattices (Fig. 3). The atom A' [as well as other atoms in the same (solid circle) sub-lattice] moves to A in order to readjust the lengths AB, AC, and AD such that atom A reaches equilibrium. The lattice structure accounting for the shift vector $\boldsymbol{\zeta}$ is marked by the solid lines in Fig. 3. Accordingly, the vector $\boldsymbol{r}_{AB}$ between two atoms A and B from different sub-lattices after the deformation is given by

$$\boldsymbol{r}_{AB} = \boldsymbol{F} \cdot \boldsymbol{r}_{AB}^{(0)} + \boldsymbol{\zeta}, \tag{17}$$

i.e., a sum of the shift vector $\boldsymbol{\zeta}$ and that associated with the Cauchy–Born rule (16). Eq. (17) has also accounted for the effect of finite deformation, contrary to Heyd et al.'s (1997) and Yang et al.'s (1999) infinitesimal deformation analyses. Its length becomes

$$r_{AB} = \sqrt{\boldsymbol{r}_{AB} \cdot \boldsymbol{r}_{AB}} = \sqrt{\boldsymbol{\zeta} \cdot \boldsymbol{\zeta} + 2\boldsymbol{\zeta} \cdot \boldsymbol{F} \cdot \boldsymbol{r}_{AB}^{(0)} + \boldsymbol{r}_{AB}^{(0)} \cdot (\boldsymbol{I} + 2\boldsymbol{E}) \cdot \boldsymbol{r}_{AB}^{(0)}}, \tag{18}$$

where $\boldsymbol{E}$ is the Lagrangian strain tensor. For comparison, the length of a vector between atoms (e.g., B and C) in the same sub-lattice is given by

$$r_{BC} = \sqrt{\boldsymbol{r}_{BC}^{(0)} \cdot (\boldsymbol{I} + 2\boldsymbol{E}) \cdot \boldsymbol{r}_{BC}^{(0)}}. \tag{19}$$

It is important to point out that, in order to obtain the bond length between atoms on a CNT, we must map the "unrolled" plane in Fig. 3 back to the three-dimensional configuration of the CNT. In fact, this is exactly the same as (6)–(13) in Section 2.2, except that the lengths a_1, a_2, a_3, a_4, and a_5 are replaced by $\boldsymbol{r}_{BC}$, $\boldsymbol{r}_{DC}$, $\boldsymbol{r}_{BD}$, $\boldsymbol{r}_{AB}$, and $\boldsymbol{r}_{AC}$, respectively. These lengths now depend on both the Lagrangian strain $\boldsymbol{E}$ and the shift vector $\boldsymbol{\zeta}$.

2.3.2. *Determination of the shift vector* $\boldsymbol{\zeta}$

It is recalled that the shift vector $\boldsymbol{\zeta}$ is introduced to ensure the equilibrium of atoms for a noncentrosymmetric lattice structure. The equilibrium of atoms is, in fact, equivalent to the minimization of energy stored in atomic bonds. Let V_{AB} denote the energy stored in the bond between atoms A and B, and V_{AB} is obtained from Brenner's (1990) interatomic potential (1) with the bond lengths and angles calculated for the three-dimensional configuration of the CNT. Therefore, V_{AB} is a function of the Lagrangian strain $\boldsymbol{E}$ and the shift vector $\boldsymbol{\zeta}$, i.e., $V_{AB} = V_{AB}(\boldsymbol{E}, \boldsymbol{\zeta})$. Similarly, we use V_{AC} and V_{AD} to denote the energy stored in bonds AC and AD. The energy for the representative atom A is given by $\frac{1}{2}[V_{AB} + V_{AC} + V_{AD}]$, where only the nearest-neighbor atomic interaction is accounted for. The shift vector $\boldsymbol{\zeta}$ is determined by minimizing the energy per atom with respect to $\boldsymbol{\zeta}$,

$$\frac{\partial}{\partial \boldsymbol{\zeta}} [V_{AB}(\boldsymbol{E}, \boldsymbol{\zeta}) + V_{AC}(\boldsymbol{E}, \boldsymbol{\zeta}) + V_{AD}(\boldsymbol{E}, \boldsymbol{\zeta})] = 0. \tag{20}$$

This gives $\boldsymbol{\zeta}$ as an implicit function of the Lagrangian strain $\boldsymbol{E}$, i.e., $\boldsymbol{\zeta}=\boldsymbol{\zeta}(\boldsymbol{E})$. Therefore, the energy stored in each bond (e.g., AB) can be expressed as $V_{AB}[\boldsymbol{E},\boldsymbol{\zeta}(\boldsymbol{E})]$.

2.3.3. The second Piola–Kirchhoff stress tensor

We may define the strain energy density W on the continuum level as the energy per unit area of the CNT surface, i.e.,

$$W = W[\boldsymbol{E},\boldsymbol{\zeta}(\boldsymbol{E})] = \frac{V_{AB}[\boldsymbol{E},\boldsymbol{\zeta}(\boldsymbol{E})] + V_{AC}[\boldsymbol{E},\boldsymbol{\zeta}(\boldsymbol{E})] + V_{AD}[\boldsymbol{E},\boldsymbol{\zeta}(\boldsymbol{E})]}{2\Omega_{\varepsilon}}, \tag{21}$$

where Ω_{ε} is the surface area per atom for an undeformed CNT, and is given by $\Omega_{\varepsilon} = \sqrt{s(s-a_1)(s-a_2)(s-a_3)}$, $s=(a_1+a_2+a_3)/2$, and a_1, a_2 and a_3 are shown in Fig. 2b for the undeformed CNT.

The second Piola–Kirchhoff stress is the work conjugate of the Lagrangian strain $\boldsymbol{E}$, and is therefore given by

$$\boldsymbol{T} = \frac{\partial W}{\partial \boldsymbol{E}}, \tag{22}$$

where the condition $\partial W/\partial\boldsymbol{\zeta} = 0$ which is equivalent to (20) has been used.

2.3.4. Atom positions on a single wall carbon nanotube under tension/torsion

2.3.4.1. Tension A single wall CNT is subject to Lagrangian strain E_{ZZ} in the axial direction and a vanishing shear strain $E_{\Theta Z}(=E_{Z\Theta})$. The second Piola–Kirchhoff stress $T_{\Theta\Theta}$ in the circumferential direction vanishes in simple tension

$$T_{\Theta\Theta} = 0, \tag{23}$$

which gives an implicit equation to determine the Lagrangian strain $E_{\Theta\Theta}$ in the circumferential direction in terms of E_{ZZ}. In fact, for each given E_{ZZ}, three variables, namely shift vector $\boldsymbol{\zeta}$ (ζ_Z and ζ_Θ) and $E_{\Theta\Theta}$, are determined together from (20), (22), and (23) by the following three equations

$$\frac{\partial W[E_{ZZ},E_{\Theta\Theta},\boldsymbol{\zeta}]}{\partial\zeta_Z} = \frac{\partial W[E_{ZZ},E_{\Theta\Theta},\boldsymbol{\zeta}]}{\partial\zeta_\Theta} = \frac{\partial W[E_{ZZ},E_{\Theta\Theta},\boldsymbol{\zeta}]}{\partial E_{\Theta\Theta}} = 0. \tag{24}$$

The atom positions on the CNT under tension are then obtained from (17), where the non-vanishing components of $\boldsymbol{F}$ are $F_{ZZ}=\sqrt{1+2E_{ZZ}}$ and $F_{\Theta\Theta}=\sqrt{1+2E_{\Theta\Theta}}$. The commonly used engineering strain in tension, ε, is given by $\varepsilon=F_{ZZ}-1=\sqrt{1+2E_{ZZ}}-1$.

It should be pointed out that the underlying principle of the above approach to determine the atom positions in a uniformly deformed CNT is the same as that of molecular mechanics calculations based on Brenner's (1990) interatomic potential. Fig. 4 shows the bond lengths $\boldsymbol{r}_{AB}$ and $\boldsymbol{r}_{AD}$ in a (10,0) CNT versus the engineering strain ε predicted by the present shift vector method and by molecular mechanics. Here AD is the bond parallel to the tube axis, and AB represents two other bonds. The molecular mechanics calculation involves a (10,0) CNT with 1400 atoms, and the atom positions are determined by energy minimization. It is observed that the present shift vector method gives the same results with the molecular mechanics calculations.

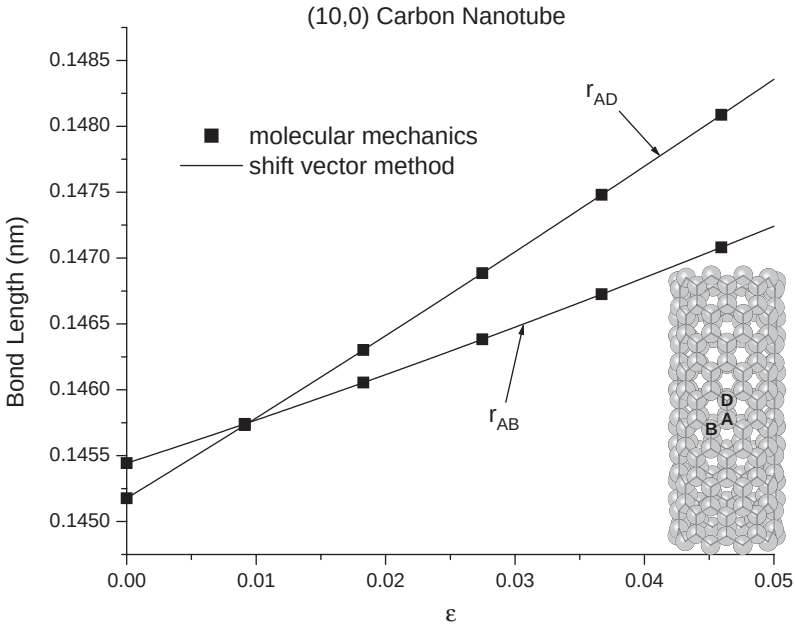

Fig. 4. The bond lengths versus the engineering strain ε for a (10, 0) carbon nanotube in tension. Results for both molecular mechanics calculations and the present shift vector method are shown.

2.3.4.2. Torsion Let κ denote the twist (angle of rotation per unit length) for a CNT under torsion, and R and r the CNT radius prior to and after torsion, respectively. The cylindrical coordinates (R, Θ, Z) of a material point on the CNT prior to torsion become (r, θ, z) after torsion, where $\theta = \Theta + \kappa Z$, and $z = Z$. The base vectors $\boldsymbol{e}_r$, $\boldsymbol{e}_\theta$, and $\boldsymbol{e}_z$ in the cylindrical coordinates for the deformed CNT are related to their counterparts $\boldsymbol{e}_R$, $\boldsymbol{e}_\Theta$, and $\boldsymbol{e}_Z$ prior to torsion by $\boldsymbol{e}_r = \cos\kappa Z\boldsymbol{e}_R + \sin\kappa Z\boldsymbol{e}_\Theta$, $\boldsymbol{e}_\theta = -\sin\kappa Z\boldsymbol{e}_R + \cos\kappa Z\boldsymbol{e}_\Theta$, and $\boldsymbol{e}_z = \boldsymbol{e}_Z$. The deformation gradient for a material point moving from $R\boldsymbol{e}_R + Z\boldsymbol{e}_Z$ (prior to deformation) to $r\boldsymbol{e}_r + z\boldsymbol{e}_z$ (after deformation) is given by

$$\begin{aligned}\boldsymbol{F} &= \frac{r}{R}\boldsymbol{e}_\theta\boldsymbol{e}_\Theta + \kappa r\boldsymbol{e}_\theta\boldsymbol{e}_Z + \boldsymbol{e}_z\boldsymbol{e}_Z \\ &= \frac{r}{R}(-\sin\kappa Z\boldsymbol{e}_R + \cos\kappa Z\boldsymbol{e}_\Theta)\boldsymbol{e}_\Theta + \kappa r(-\sin\kappa Z\boldsymbol{e}_R + \cos\kappa Z\boldsymbol{e}_\Theta)\boldsymbol{e}_Z + \boldsymbol{e}_Z\boldsymbol{e}_Z, \end{aligned} \quad (25)$$

where the radius r of the deformed CNT remains to be determined for each given κ. The Lagrangian strain $\boldsymbol{E}$ is found from (15) as

$$\boldsymbol{E} = \frac{1}{2}\left(\frac{r^2}{R^2} - 1\right)\boldsymbol{e}_\Theta\boldsymbol{e}_\Theta + \frac{\kappa}{2}\frac{r^2}{R}(\boldsymbol{e}_\Theta\boldsymbol{e}_Z + \boldsymbol{e}_Z\boldsymbol{e}_\Theta) + \frac{1}{2}\kappa^2 r^2\boldsymbol{e}_Z\boldsymbol{e}_Z. \quad (26)$$

Here the non-vanishing normal strains $E_{\Theta\Theta}$ and E_{ZZ} result from the finite deformation. It is noted that the Lagrangian strains are given in terms of κ and the radius r of the CNT under torsion. As shown in Appendix A, equilibrium requires that the second

Piola–Kirchhoff stress $T_{\Theta\Theta}$, T_{ZZ}, and $T_{\Theta Z}(=T_{Z\Theta})$ be constants (i.e., independent of Θ and Z) in torsion, and satisfy

$$T_{\Theta\Theta} + 2\kappa R T_{\Theta Z} + \kappa^2 R^2 T_{ZZ} = 0. \tag{27}$$

The above equation, in conjunction with (22), gives an implicit equation to determine r. Similar to (24) for tension, three variables, namely, the shift vector $\boldsymbol{\zeta}$ (ζ_Z and ζ_Θ) and radius r of the deformed CNT, are determined together from (20), (22) and (27) for each given κ by the following three equations

$$\frac{\partial W(\boldsymbol{E},\boldsymbol{\zeta})}{\partial \zeta_Z} = \frac{\partial W(\boldsymbol{E},\boldsymbol{\zeta})}{\partial \zeta_\Theta} = \frac{\partial W(\boldsymbol{E},\boldsymbol{\zeta})}{\partial E_{\Theta\Theta}} + 2\kappa R \frac{\partial W(\boldsymbol{E},\boldsymbol{\zeta})}{\partial E_{\Theta Z}} + \kappa^2 R^2 \frac{\partial W(\boldsymbol{E},\boldsymbol{\zeta})}{\partial E_{ZZ}} = 0. \tag{28}$$

The atom positions on the CNT under torsion are then obtained from (17).

2.3.4.3. Combined tension and torsion We investigate a single wall CNT subject to combined tension and torsion characterized by the axial (engineering) strain ε and twist κ. The deformation gradient can be obtained similar to (25) as

$$\boldsymbol{F} = \frac{r}{R}(-\sin\kappa Z\boldsymbol{e}_R + \cos\kappa Z\boldsymbol{e}_\Theta)\boldsymbol{e}_\Theta + \kappa r(-\sin\kappa Z\boldsymbol{e}_R + \cos\kappa Z\boldsymbol{e}_\Theta)\boldsymbol{e}_Z + (1+\varepsilon)\boldsymbol{e}_Z\boldsymbol{e}_Z. \tag{29}$$

It is straightforward to verify that, for $\kappa = 0$, the above expression degenerates to that for tension, with r/R being $F_{\Theta\Theta}$. The Lagrangian strain for the combined tension/torsion is given in terms of ε, κ and r by

$$\boldsymbol{E} = \frac{1}{2}\left(\frac{r^2}{R^2} - 1\right)\boldsymbol{e}_\Theta\boldsymbol{e}_\Theta + \frac{\kappa}{2}\frac{r^2}{R}(\boldsymbol{e}_\Theta\boldsymbol{e}_Z + \boldsymbol{e}_Z\boldsymbol{e}_\Theta) + \frac{1}{2}(\kappa^2 r^2 + 2\varepsilon + \varepsilon^2)\boldsymbol{e}_Z\boldsymbol{e}_Z. \tag{30}$$

It can be shown that (27) still holds for the combined tension and torsion, and it is the implicit equation to determine the radius r of the deformed CNT for given κ and ε. Once the shift vector $\boldsymbol{\zeta}$ is obtained from (20), the atom positions on a CNT subject to combined tension and torsion are determined.

3. The tight-binding calculation of band gap for a single wall carbon nanotube

The semi-empirical tight-binding method uses the bonding electron orbitals associated with each of the atoms in a semiconductor material to represent the energetics of the structure. The eigenstates of the Hamiltonian of the material are written in an atomic-like basis set, $\{\phi_{i\alpha}\}$, and the exact many-body Hamiltonian operator is replaced with a parameterized Hamiltonian matrix. For an atomic structure such as a CNT, the tight-binding method provides the energy states corresponding to different bonding and anti-bonding electron orbital states. These energy states can be used to determine the electrical properties of the structure; combined with a repulsive empirical pair-wise potential, the electron states can also be used to compute the mechanical properties of the structure. Here only the electronic properties are of interest, since the

atomic positions and energetics of the system are computed from the method described in the previous sections.

The tight-binding method of modeling materials lies between the very accurate, very expensive ab initio methods and the fast but limited empirical methods (e.g., see Goringe et al., 1997), such as the Brenner potential used in the previous sections. When compared with ab initio methods, tight-binding is typically two to three orders of magnitude faster, but suffers from a reduction in transferability due to the approximations made; when compared with empirical methods, tight-binding is two to three orders of magnitude slower, but the quantum mechanical nature of bonding is retained, ensuring that the angular nature of bonding is correctly described in far from equilibrium structures.

For materials whose structure has translational symmetry, it is convenient to use the k-space tight-binding method, which makes use of the symmetry to significantly reduce the computational effort. The k-space tight-binding method has been used to study the electrical property of undeformed CNTs (e.g., Saito et al., 1998). However, the focus of this section is the tight-binding calculation for the deformed CNTs. Fig. 5 shows the lattice structure of the deformed CNT, which can be divided into unit cells (marked by the dashed lines in Fig. 5a) containing two inequivalent atoms. The deformation of a CNT is completely characterized by three vectors $\boldsymbol{d}_1$, $\boldsymbol{d}_2$, and $\boldsymbol{d}_3$ from the representative atom A to its three nearest-neighbor atoms B, C, and D (Fig. 5b), where $\boldsymbol{d}_1$, $\boldsymbol{d}_2$, and $\boldsymbol{d}_3$ are given in terms of the deformation gradient $\boldsymbol{F}$ and the shift vector $\boldsymbol{\zeta}$ via (17). Since the unit cell has two carbon atoms and each atom has four outer valence electron orbitals, the tight-binding Hamiltonian is an 8×8 matrix, and is given by

$$\boldsymbol{H}(\boldsymbol{k})=\begin{bmatrix} \varepsilon_s & 0 & 0 & 0 & H^{ss} & H^{sx} & H^{sy} & H^{sz} \\ 0 & \varepsilon_p & 0 & 0 & -H^{sx} & H^{xx} & H^{yx} & H^{zx} \\ 0 & 0 & \varepsilon_p & 0 & -H^{sy} & H^{xy} & H^{yy} & H^{zy} \\ 0 & 0 & 0 & \varepsilon_p & -H^{sz} & H^{xz} & H^{yz} & H^{zz} \\ H^{ss^*} & -H^{sx^*} & -H^{sy^*} & -H^{sz^*} & \varepsilon_s & 0 & 0 & 0 \\ H^{sx^*} & H^{xx^*} & H^{xy^*} & H^{xz^*} & 0 & \varepsilon_p & 0 & 0 \\ H^{sy^*} & H^{yx^*} & H^{yy^*} & H^{yz^*} & 0 & 0 & \varepsilon_p & 0 \\ H^{sz^*} & H^{zx^*} & H^{zy^*} & H^{zz^*} & 0 & 0 & 0 & \varepsilon_p \end{bmatrix}, \tag{31}$$

where only the nearest-neighbor interaction is considered; $\boldsymbol{k}$ is the wave vector; ε_s and ε_p are the orbital energy of s and p levels, respectively; $H^{\alpha\beta}$ terms represent interactions between orbitals of neighboring atoms, $H^{\alpha\beta^*}$ is the complex conjugate of $H^{\alpha\beta}$, and $H^{\alpha\beta}$ are given in terms of the wave vector $\boldsymbol{k}$ by

$$H^{ss}=V_{ss\sigma}(d_1)\mathrm{e}^{\mathrm{i}\boldsymbol{k}\cdot\boldsymbol{d}_1}+V_{ss\sigma}(d_2)\mathrm{e}^{\mathrm{i}\boldsymbol{k}\cdot\boldsymbol{d}_2}+V_{ss\sigma}(d_3)\mathrm{e}^{\mathrm{i}\boldsymbol{k}\cdot\boldsymbol{d}_3},$$

$$H^{sx}=l_1V_{sp\sigma}(d_1)\mathrm{e}^{\mathrm{i}\boldsymbol{k}\cdot\boldsymbol{d}_1}+l_2V_{sp\sigma}(d_2)\mathrm{e}^{\mathrm{i}\boldsymbol{k}\cdot\boldsymbol{d}_2}+l_3V_{sp\sigma}(d_3)\mathrm{e}^{\mathrm{i}\boldsymbol{k}\cdot\boldsymbol{d}_3},$$

$$H^{sy}=m_1V_{sp\sigma}(d_1)\mathrm{e}^{\mathrm{i}\boldsymbol{k}\cdot\boldsymbol{d}_1}+m_2V_{sp\sigma}(d_2)\mathrm{e}^{\mathrm{i}\boldsymbol{k}\cdot\boldsymbol{d}_2}+m_3V_{sp\sigma}(d_3)\mathrm{e}^{\mathrm{i}\boldsymbol{k}\cdot\boldsymbol{d}_3},$$

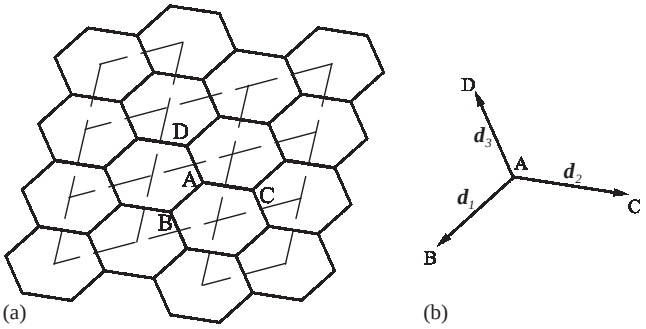

Fig. 5. The representative atom A and its three nearest neighbor atoms B, C and D for the k-space tight-binding calculation. (a) Unit cells and (b) atom positions.

$$H^{sz} = n_1 V_{sp\sigma}(d_1)\mathrm{e}^{\mathrm{i}\boldsymbol{k}\cdot\boldsymbol{d}_1} + n_2 V_{sp\sigma}(d_2)\mathrm{e}^{\mathrm{i}\boldsymbol{k}\cdot\boldsymbol{d}_2} + n_3 V_{sp\sigma}(d_3)\mathrm{e}^{\mathrm{i}\boldsymbol{k}\cdot\boldsymbol{d}_3},$$

$$H^{xx} = fxx(1)\mathrm{e}^{\mathrm{i}\boldsymbol{k}\cdot\boldsymbol{d}_1} + fxx(2)\mathrm{e}^{\mathrm{i}\boldsymbol{k}\cdot\boldsymbol{d}_2} + fxx(3)\mathrm{e}^{\mathrm{i}\boldsymbol{k}\cdot\boldsymbol{d}_3},$$

$$H^{xy} = fxy(1)\mathrm{e}^{\mathrm{i}\boldsymbol{k}\cdot\boldsymbol{d}_1} + fxy(2)\mathrm{e}^{\mathrm{i}\boldsymbol{k}\cdot\boldsymbol{d}_2} + fxy(3)\mathrm{e}^{\mathrm{i}\boldsymbol{k}\cdot\boldsymbol{d}_3},$$

$$H^{xz} = fxz(1)\mathrm{e}^{\mathrm{i}\boldsymbol{k}\cdot\boldsymbol{d}_1} + fxz(2)\mathrm{e}^{\mathrm{i}\boldsymbol{k}\cdot\boldsymbol{d}_2} + fxz(3)\mathrm{e}^{\mathrm{i}\boldsymbol{k}\cdot\boldsymbol{d}_3}, \tag{32}$$

where $d_i = |\boldsymbol{d}_i|$ $(i = 1,2,3)$ are the lengths of the deformed bonds, l_i, m_i and n_i are the direction cosines of $\boldsymbol{d}_i$ in a Cartesian coordinate system (x, y, z), and the prefactors $fxx(i)$, $fxy(i)$ and $fxz(i)$ are given by

$$fxx(i) = l_i^2 V_{pp\sigma}(d_i) + (1 - l_i^2)V_{pp\pi}(d_i),$$

$$fxy(i) = l_i m_i V_{pp\sigma}(d_i) - l_i m_i V_{pp\pi}(d_i),$$

$$fxz(i) = l_i n_i V_{pp\sigma}(d_i) - l_i n_i V_{pp\pi}(d_i). \tag{33}$$

Other prefactors (e.g., f_{yx}) can be obtained similar to (33). The other matrix elements H^{yx}, H^{yy}, H^{yz}, H^{zx}, H^{zy}, and H^{zz} in (31) are then determined following (32).

The hopping parameters $V_{ss\sigma}$ and $V_{sp\sigma}$ in (32) and $V_{pp\sigma}$ and $V_{pp\pi}$ in (33) scale with interatomic separation as follows

$$\begin{Bmatrix} V_{ss\sigma}(r) \\ V_{sp\sigma}(r) \\ V_{pp\sigma}(r) \\ V_{pp\pi}(r) \end{Bmatrix} = \begin{Bmatrix} V_{ss\sigma}^{(0)} \\ V_{sp\sigma}^{(0)} \\ V_{pp\sigma}^{(0)} \\ V_{pp\pi}^{(0)} \end{Bmatrix} s(r). \tag{34}$$

Goodwin et al. (1989) suggested the function $s(r)$ as

$$s(r) = (r_0/r)^n \exp\{n\lfloor -(r/r_c)^{n_c} + (r_0/r_c)^{n_c}\rfloor\}. \tag{35}$$

Xu et al. (1992) determined all parameters in (31), (34) and (35) for carbon as

$$\varepsilon_s = -2.99 \text{ eV}, \quad \varepsilon_p = 3.71 \text{ eV},$$

$$V_{ss\sigma_0} = -5.0 \text{ eV}, \quad V_{sp\sigma_0} = 4.7 \text{ eV}, \quad V_{pp\sigma_0} = 5.5 \text{ eV}, \quad V_{pp\pi_0} = -1.55 \text{ eV},$$

$$n = 2.0, \quad n_c = 6.5, \quad r_c = 2.18 \text{ Å}, \quad r_0 = 1.536329 \text{ Å}. \tag{36}$$

The wave vector $\boldsymbol{k}$ in the Hamiltonian matrix (31) is quantized because of the periodic boundary condition in the circumferential direction for a CNT, and is given by

$$\boldsymbol{k} = k_t \frac{\boldsymbol{K}}{|\boldsymbol{K}_2|} + \mu \boldsymbol{K}_1 \quad \left(\mu = 0, \ldots, N-1, \text{ and } -\frac{\pi}{|\boldsymbol{T}|} < k_t < \frac{\pi}{|\boldsymbol{T}|} \right), \tag{37}$$

where N is the number of hexagons in the area of $|\boldsymbol{C}_h \times \boldsymbol{T}|$, $\boldsymbol{K}_1 = 2\pi \boldsymbol{C}_h / |\boldsymbol{C}_h|^2$ and $\boldsymbol{K}_2 = 2\pi \boldsymbol{T} / |\boldsymbol{T}|^2$ are the reciprocal lattice vectors, $\boldsymbol{C}_h$ and $\boldsymbol{T}$ are the chiral and translational vectors of the deformed CNT.

For each wave vector $\boldsymbol{k}$ in (37), we solve the energy eigenstates by diagonalizing the Hamiltonian matrix in (31). Once the energy eigenstates are determined for all wave vectors, the energy dispersion relations for σ and π bands are obtained, which give the band gap of the deformed CNT. Fig. 6 shows an example of the energy dispersion relations for a zigzag (10,0) CNT prior to deformation. The energy states are shown versus the axial component k_t of the wave vector $\boldsymbol{k}$ for all quantized μ in (37). The band gap is the difference between the highest filled band and the lowest

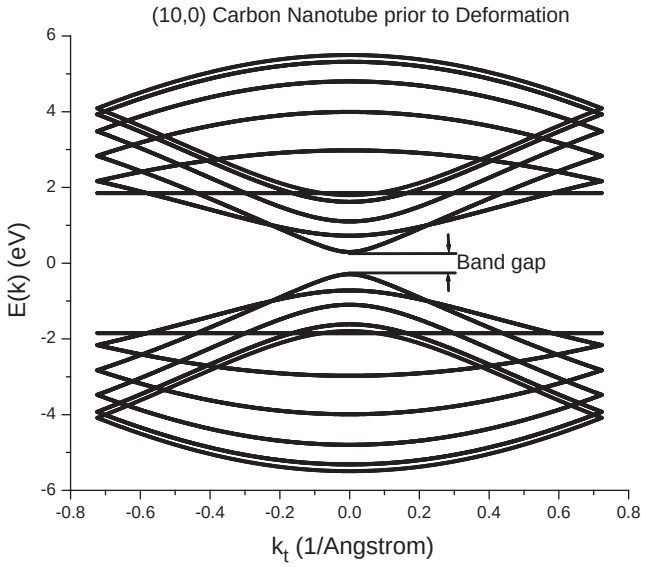

Fig. 6. The energy dispersion relations for a zigzag (10,0) carbon nanotube prior to deformation, which shows a finite band gap.

unfilled band, and is clearly marked in Fig. 6. The exact filling of states, usually related to temperature through the Fermi-Dirac distribution, is not of interest here since the energetics and mechanical behavior of the system is already known from the continuum based empirical potential approach described in the previous sections. Instead, the band gap is viewed simply as a measure of whether the CNT is electrically conducting; zero band gap corresponds to electrically conducting materials, while a non-vanishing, finite band gap generally corresponds to semi-conducting materials.

4. The band gap of a carbon nanotube subject to tension/torsion

It has been established (e.g., Saito et al., 1998) that an undeformed CNT is electrically conducting (i.e., band gap $= 0$) if the chirality satisfies $n - m = 3l$ ($l = 0, 1, 2, \ldots$); otherwise a CNT is semi-conducting (i.e., band gap > 0). According to this commonly used criterion, we select a group of conducting CNTs [armchair (5,5), zigzag (9,0), and chiral (9,6)] and a group of semi-conducting CNTs [zigzag (10,0) and chiral (6,4)]. We investigate the effect of deformation on the band gap for these CNTs under tension, torsion, or combined tension/torsion.

4.1. Tension

Fig. 7 shows the band gap versus the engineering strain ε for a zigzag (9,0) CNT under tension. It includes two curves that correspond to the atom position calculations with and without the shift vector $\boldsymbol{\zeta}$ introduced in Section 2. It is clearly observed that the shift vector $\boldsymbol{\zeta}$ has an important effect on the band gap. For a large strain $\varepsilon = 10\%$,

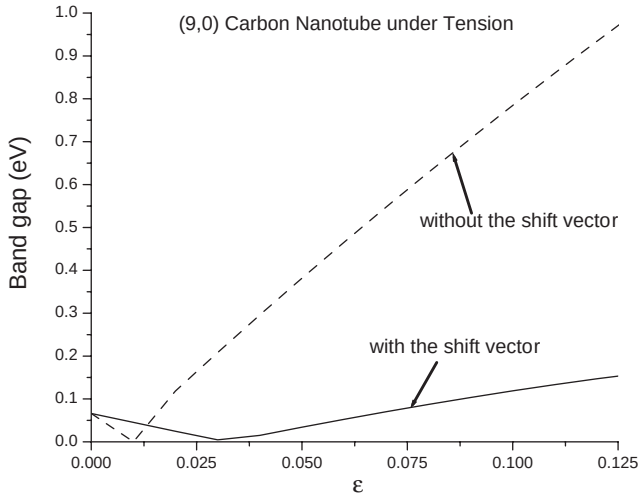

Fig. 7. The band gap versus the tensile strain ε for a (9,0) carbon nanotube under tension. The results are shown for calculations with and without the shift vector.

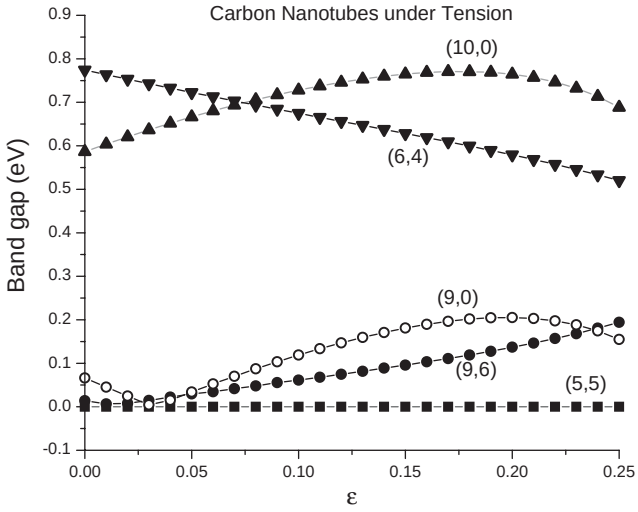

Fig. 8. The band gap versus the tensile strain ε accounting for the shift vector for various carbon nanotubes under tension.

the calculation without the shift vector significantly overestimates the band gap by a factor of 6. Yang et al.'s (1999) tight-binding calculations for the same (9,0) CNT also showed that the band gap based on the simple deformation pattern (i.e., without the shift vector) is overestimated as compared to that based on molecular mechanics calculation of atom positions.

Fig. 8 shows the band gap versus the engineering strain ε for (5,5), (9,0), (9,6), (10,0), and (6,4) CNTs. The band gap for the armchair (5,5) CNT under tension remains zero. This conclusion also holds for other armchair (n,n) CNTs, i.e., they remain conducting under tension. For the conducting zigzag (9,0) and chiral (9,6) CNTs, the band gap generally increases with tension, which suggests that the conducting CNTs may become semi-conducting upon deformation. For the semi-conducting zigzag (10,0) and chiral (6,4) CNTs, the band gap displays some variation upon deformation, but it remains large.

It is observed that the zigzag (9,0) CNT shows a small band gap even prior to deformation, which seems to contradict with the prediction of vanishing band gap for $n-m=3l$. This is because the effect of CNT radius on the bond lengths and angles has not been accounted for in the above criterion. Yang et al. (1999) also showed a small band gap of the undeformed (9,0) CNT. Therefore, the widely accepted criterion $n-m=3l$ for conducting CNTs is only approximate.

4.2. Torsion

Without the shift vector, the band gap is also overestimated, as shown in Fig. 9 for an armchair (5,5) CNT under torsion. This is also consistent with Yang et al.'s (1999) tight-binding calculations for the same armchair (5,5) CNT under torsion.

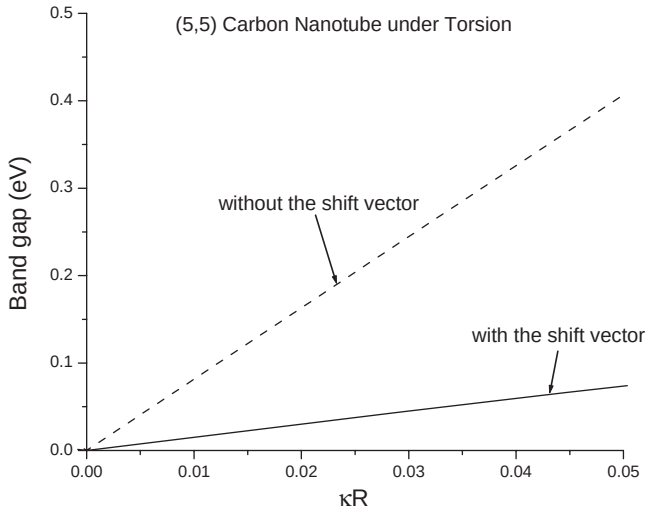

Fig. 9. The band gap versus the normalized twist κR for a (5,5) carbon nanotube (CNT) under torsion, where κ is the twist (rotation per unit length) and R is the radius of the CNT. The results are shown for calculations with and without the shift vector.

Fig. 10 shows the band gap versus the normalized twist, κR, for (5,5), (9,0), (9,6), (10,0), and (6,4) CNTs under torsion, where R is the CNT radius prior to deformation. The twist κ can be positive or negative, depending on the direction of torsion. The curves are symmetric about $\kappa R = 0$ for zigzag and armchair CNTs, but are unsymmetric for chiral CNTs. Contrary to tension, the band gap of armchair (5,5) CNT is not zero anymore once torsion is imposed; it increases with the twist $|\kappa|$, but starts to decrease when $|\kappa|$ is very large. The conducting chiral (9,6) CNT displays similar behavior, but its band gap is unsymmetric about $\kappa R = 0$. However, the band gap for the zigzag (9,0) CNT decreases at small twist, but then increases rapidly with deformation. For two semi-conducting (10,0) and (6,4) CNTs, the band gap remains large upon deformation, which is consistent with the observation for these CNTs under tension (Fig. 8).

4.3. Combined tension/torsion

We have also obtained the band gap for CNTs under combined tension/torsion. Figs. 11a, c, and e show the distribution of band gap versus the tensile (engineering) strain ε and normalized twist κR for (5,5), (9,0), and (9,6) CNTs, respectively. Only $\kappa R \geqslant 0$ is shown for (5,5) and (9,0) CNTs due to symmetry. It is observed that the band gap is non-zero almost over the entire domain; only around very isolated curves does the band gap vanish. This is clearly observed from the contour plot of band gap in Figs. 11b, d and f for the same CNTs. The isolated curves for vanishing band gap are marked by the white dashed lines. Therefore, even though these three CNTs are considered as conducting by the simple criterion $n - m = 3l$ $(l = 0, 1, 2, \ldots)$, their band gap will most likely become finite and the conducting CNTs will become semi-conducting once

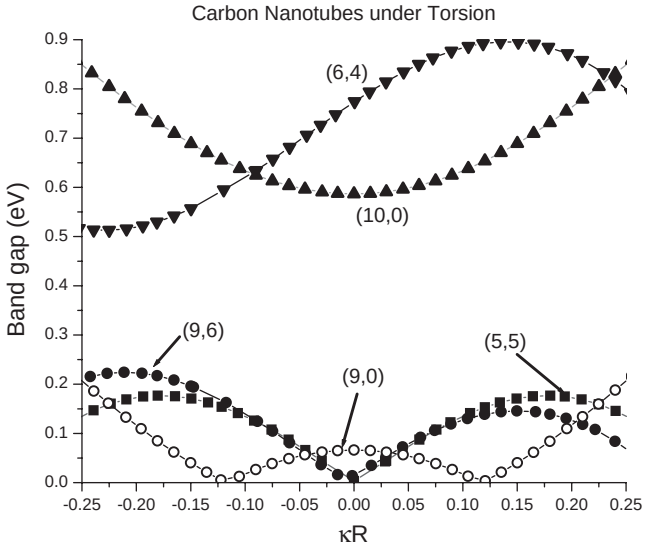

Fig. 10. The band gap versus the normalized twist κR accounting for the shift vector for various carbon nanotubes (CNT), where κ is the twist (rotation per unit length) and R is the radius of the CNT. The results are shown for calculations with and without the shift vector.

the deformation is imposed. In fact, a similar conclusion has been reached in Tombler et al.'s (2000) experiments, which showed that the electrical conductance of a CNT may be reduced by two orders of magnitude due to deformation.

The distribution of band gap is shown in Fig. 12 for the zigzag (10,0) and chiral (6,4) semi-conducting CNTs. The band gap in general is significantly larger than that in Fig. 11, and never reaches zero. Therefore, semi-conducting CNTs under tension/torsion cannot become conductors. It is also observed that the variation of band gap is relatively small; the largest band gap is no more than twice the smallest one. Accordingly, the conductance change of semi-conducting CNTs upon relatively uniform deformation is not expected to be two orders of magnitude, contrary to Tombler et al.'s (2000) experiments for conducting CNTs. In fact, the experiment of Paulson et al. (1999) did not show a significant change in the conductance.

5. Discussion

It is convenient to show the effects of deformation on band gap in the form of the maps shown in Figs. 7–12, but the effects of band filling and temperature on the electrical properties of the CNTs should also be considered. Since the energetics and mechanical properties of the CNTs are already computed here using a continuum implementation of the Brenner potential, it is not necessary to compute the electronic and total energies of the CNTs using the tight-binding results. Thus, it is not necessary to consider the filling of the available electron states such as those shown in Fig. 6

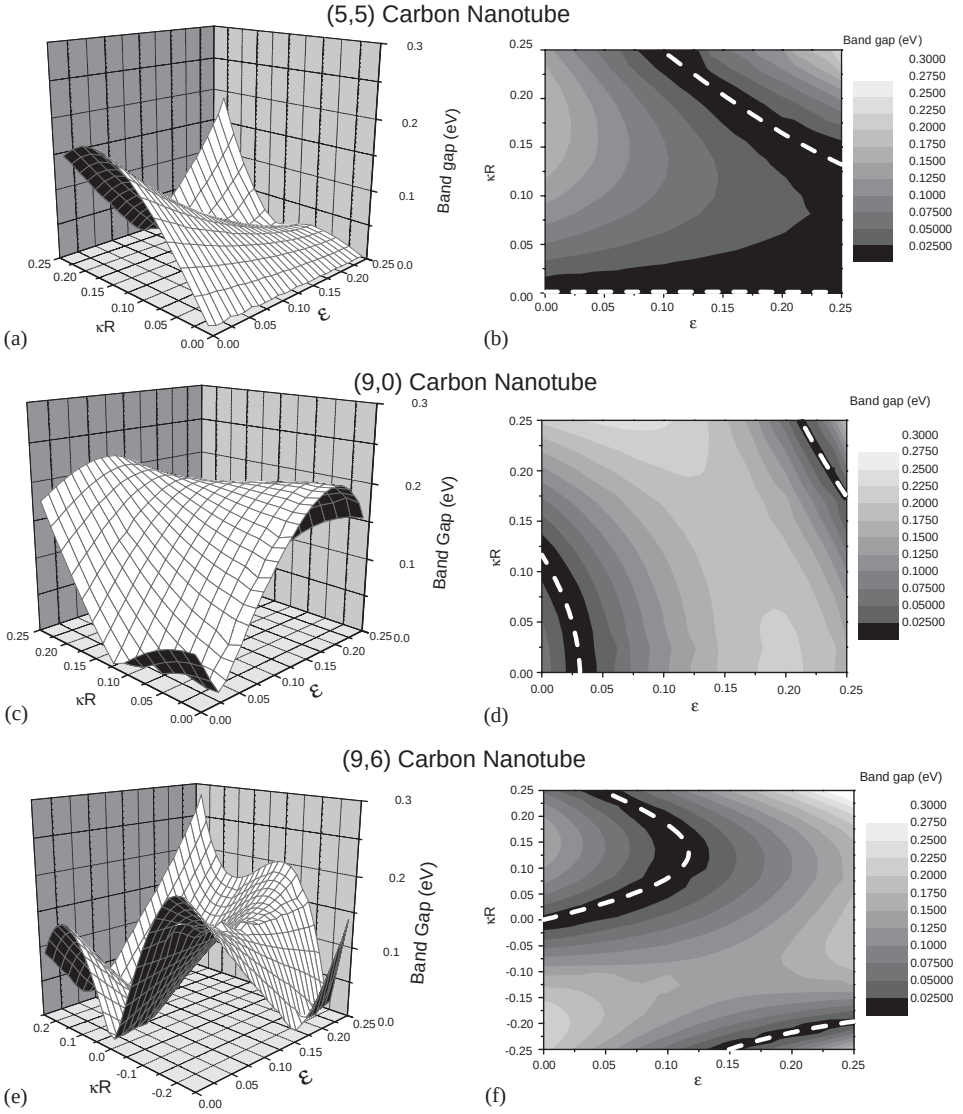

Fig. 11. The band gap versus the tensile strain ε and normalized twist κR for three conducting carbon nanotubes (CNT) under combined tension/torsion; (a) (5,5); (c) (9,0); (e) (9,6). The contour plots of band gap for the same three conducting CNTs are shown in (b), (d) and (f). The CNTs for loadings inside the black regions are conducting at room temperature.

for the (10,0) CNT. Since the details of band filling and a tight-binding based total energy are not of interest here, it is reasonable to use the tight-binding approach even for CNTs approaching metallic behavior.

However, in the context of the tight-binding method, it is through the filling of the computed electronic states that temperature effects are introduced. Also, temperature

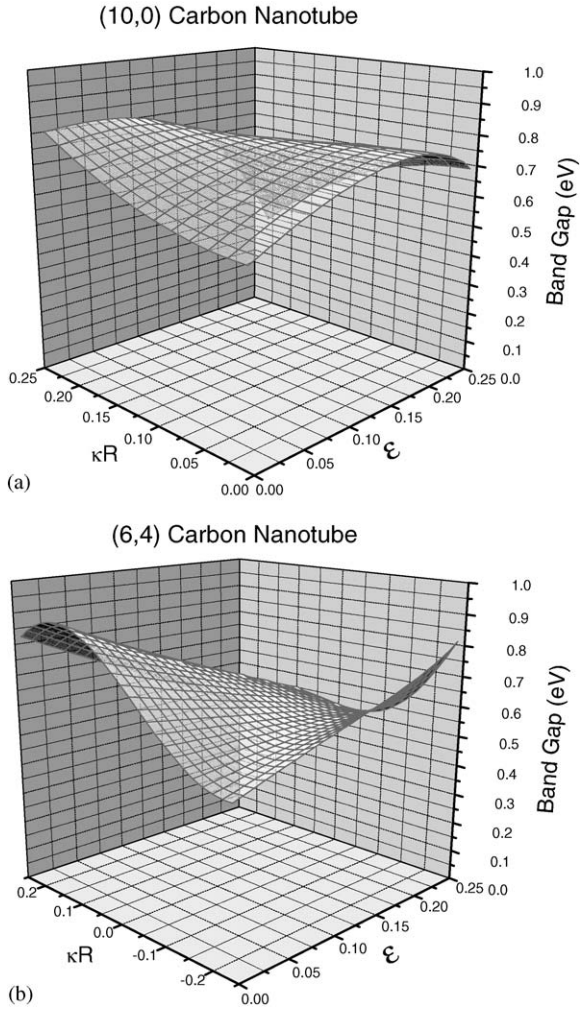

Fig. 12. The band gap versus the tensile strain ε and normalized twist κR for two semi-conducting carbon nanotubes under combined tension/torsion: (a) (10,0) and (b) (6,4).

effects set an important energy scale (approximately 0.025 eV at room temperature): thermal energy is one mechanism by which charge carriers may be excited across the energy band gap to lead to a finite conductance in a material with a nonzero energy band gap. This effect is quantified as follows.

Consider the energy vs. wave vector dispersion relation shown in Fig. 6 for the zigzag (10,0) CNT. The energy levels in the plot can be summed over the possible k-points and smoothed by a small arbitrary Gaussian broadening function to illustrate the density of states as a continuous function of energy, $\rho(E)$, as shown in Fig. 13. The density of states clearly shows the band gap of approximately 0.6 eV. The electronic

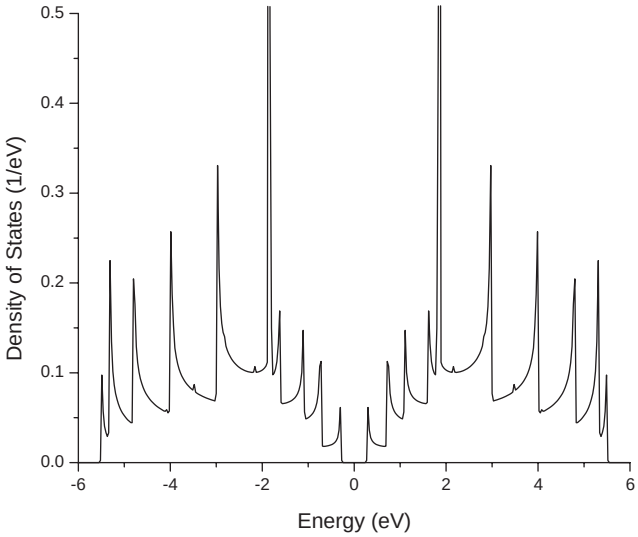

Fig. 13. The density of states versus the energy for a (10,0) carbon nanotube.

portion of the total cohesive energy would then be computed by

$$E_{el} = \int_0^{E_f} E\rho(E)\,\mathrm{d}E, \tag{38}$$

where E_f is the Fermi energy in the material. The filling of the available energy levels would be determined by the temperature dependent Fermi-Dirac distribution function $f_{\mathrm{FD}}(E, E_f, T)$, which is given by

$$f_{\mathrm{FD}} = \frac{1}{1 + \exp\left(\frac{E - E_f}{kT}\right)}, \tag{39}$$

where k is the Boltzmann constant. This distribution function represents the filling of some of the lowest conduction band states, otherwise unoccupied at zero temperature, by some of the highest valence band electrons thermally excited by temperature T. With finite temperature treated in this manner, the conductance of the CNT can be approximated using the Landauer model, given some estimate of the nature of the electrical contacts to either end of the CNT under consideration (Landauer, 1970; Chico et al., 1996). However, for the purposes of the present study, the band gap determined strictly from the zero-temperature tight-binding energy band structure is considered to be a reasonable relative measure of the electronic behavior of the deformed CNTs. Thus, finite temperature is viewed here as a basis for a physical energy scale through which to interpret the deformation-band gap maps. The thermal energy kT at room temperature is 0.025 eV, and is denoted in the contour plots in Fig. 11b, d, and f as the region in black.

6. Concluding remarks

We have developed a simple and accurate method to study the effect of mechanical deformation on the electrical properties of single wall carbon nanotubes (CNT). The atom positions prior to and after deformation are determined by the continuum analysis based on the interatomic potential. Once the atom positions are known, the band gap of the CNT is then calculated via the k-space tight-binding method for CNTs subject to tension, torsion, and combined tension/torsion. We have reached the following conclusions in the present study.

(1) Some prior analyses have assumed that carbon atoms on a CNT subject to tension/torsion follow a simple, uniform deformation pattern. This assumption overly constrains the motion of carbon atoms, and cannot ensure their equilibrium, which leads to significant overestimation of the band gap change of the CNT due to mechanical deformation. We have introduced a shift vector to relax the motion of carbon atoms and to ensure their equilibrium. The atom positions determined by this method agree very well with that obtained from molecular mechanics calculations. The predicted band gap change is then consistent with that determined from the molecular dynamic simulations.
(2) For conducting CNTs (chirality $n-m=0,3,6,9,\ldots$), mechanical deformation may lead to a finite band gap, i.e., the conducting CNT may become a semi-conducting one. A similar conclusion has been reached in Tombler et al.'s (2000) experiment. In fact, our analysis shows that the conducting CNTs remain conducting only under very special loading conditions. For semi-conducting CNTs ($n-m=1,2,4,5,\ldots$) subject to tension/torsion, however, the band gap always remains finite such that a semi-conducting CNT never becomes a conducting one. We have also discussed the effect of temperature on the conductivity of the CNTs.

Acknowledgements

Y.H. acknowledges the support from NSF (grants 00-99909 and 01-03257), Alexander von Humboldt Foundation, Center for Advanced Study at the University of Illinois, Urbana-Champaign, the NCSA/UIUC Faculty Fellow Program, and NSFC. H.T.J. acknowledges the support of NSF grants (Career Award 02-96102 and grant 02-10131).

Appendix A

The equilibrium equation for a single wall CNT is obtained by integrating the standard three-dimensional equation $(\boldsymbol{F}\cdot\boldsymbol{T})\cdot\nabla=0$ over the nanotube thickness, where $\boldsymbol{F}$ is the deformation gradient in (29), $\boldsymbol{T}$ is the second order Piola–Kirchhoff stress, and

$$\nabla=\boldsymbol{e}_R\frac{\partial}{\partial R}+\frac{\boldsymbol{e}_\theta}{R}\frac{\partial}{\partial\theta}+\boldsymbol{e}_Z\frac{\partial}{\partial Z}$$

is the gradient operator in the reference configuration. In conjunction with the traction-free boundary condition $\boldsymbol{F}\cdot\boldsymbol{T}\cdot\boldsymbol{e}_R=0$ on the inner and outer surfaces of the CNT, the equilibrium equation becomes

$$\frac{1}{R}\frac{\partial}{\partial\Theta}(\boldsymbol{F}\cdot\boldsymbol{T})_{R\Theta}-\frac{1}{R}(\boldsymbol{F}\cdot\boldsymbol{T})_{\Theta\Theta}+\frac{\partial}{\partial Z}(\boldsymbol{F}\cdot\boldsymbol{T})_{RZ}=0, \tag{A.1a}$$

$$\frac{1}{R}(\boldsymbol{F}\cdot\boldsymbol{T})_{R\Theta}+\frac{1}{R}\frac{\partial}{\partial\Theta}(\boldsymbol{F}\cdot\boldsymbol{T})_{\Theta\Theta}+\frac{\partial}{\partial Z}(\boldsymbol{F}\cdot\boldsymbol{T})_{\Theta Z}=0, \tag{A.1b}$$

$$\frac{1}{R}\frac{\partial}{\partial\Theta}(\boldsymbol{F}\cdot\boldsymbol{T})_{Z\Theta}+\frac{\partial}{\partial Z}(\boldsymbol{F}\cdot\boldsymbol{T})_{ZZ}=0. \tag{A.1c}$$

The non-vanishing components of the second Piola–Kirchhoff stress are $T_{\Theta\Theta}$, T_{ZZ}, and $T_{\Theta Z}(=T_{Z\Theta})$, and they are independent of Θ for a CNT in tension/torsion. The equilibrium equation (A.1) projected along the base vectors $\boldsymbol{e}_r$, $\boldsymbol{e}_\theta$ and $\boldsymbol{e}_z$ in the current configuration becomes

$$F_{\theta\Theta}T_{\Theta\Theta}+F_{\theta Z}T_{\Theta Z}+\kappa R(F_{\theta\Theta}T_{\Theta Z}+F_{\theta Z}T_{ZZ})=0, \tag{A.2a}$$

$$\frac{\mathrm{d}}{\mathrm{d}Z}(F_{\theta\Theta}T_{\Theta Z}+F_{\theta Z}T_{ZZ})=0, \tag{A.2b}$$

$$\frac{\mathrm{d}}{\mathrm{d}Z}(F_{zZ}T_{ZZ})=0. \tag{A.2c}$$

The substitution of the deformation gradient in (29) into (A.2) yields

$$T_{ZZ}=\text{constant},\qquad T_{\Theta Z}=\text{constant}, \tag{A.3a}$$

$$T_{\Theta\Theta}+2\kappa RT_{\Theta Z}+\kappa^2R^2T_{ZZ}=0. \tag{A.3b}$$

References

Arroyo, M., Belytschko, T., 2002. An atomistic-based finite deformation membrane for single layer crystalline films. J. Mech. Phys. Solids 50, 1941–1977.

Bezryadin, A., Verschueren, A.R.M., Tans, S.J., Dekker, C., 1998. Multiprobe transport experiments on individual single-wall carbon nanotubes. Phys. Rev. Lett. 80 (18), 4036–4039.

Born, M., Huang, K., 1954. Dynamical Theory of the Crystal Lattices. Oxford University Press, Oxford.

Brenner, D.W., 1990. Empirical potential for hydrocarbons for use in simulating the chemical vapor deposition of diamond films. Phys. Rev. B 42, 9458–9471.

Chico, L., Benedict, L.X., Louie, S.G., Cohen, M.L., 1996. Quantum conductance of carbon nanotubes with defects. Phys. Rev. B 54 (4), 2600–2606.

Collins, P.G., Arnold, M.S., Avouris, P., 2001. Engineering carbon nanotubes and nanotube circuits using electrical breakdown. Science 292 (5517), 706–709.

Gaal, R., Salvetat, J.P., Forro, L., 2000. Pressure dependence of the resistivity of single-wall carbon nanotube ropes. Phys. Rev. B 61 (11), 7320–7323.

Goodwin, L., Skinner, A.J., Pettifor, D.G., 1989. Generating transferable tight-binding parameters-application to silicon. Europhys. Lett. 9 (7), 701–706.

Goringe, C.M., Bowler, D.R., Hernandez, E., 1997. Tight-binding modelling of materials. Rep. Prog. Phys. 60 (12), 1447–1512.

Heyd, R., Charlier, A., McRae, E., 1997. Uniaxial-stress effects on the electronic properties of carbon nanotubes. Phys. Rev. B 55 (11), 6820–6824.

Iijima, S., 1991. Helical microtubules of graphitic carbon. Nature 354 (6348), 56–58.

Johnson, H.T., Phillips, R., Freund, L.B., 1999. Electronic structure boundary value problems without all of the atoms. Mater. Res. Soc. Symp. Proc. 538, 479–484.

Landauer, R., 1970. Electrical resistance of disorder one-dimensional lattices. Philos. Mag. 21, 863–867.

Liu, L., Jayanthi, C.S., Tang, M.J., Wu, S.Y., Tombler, T.W., Zhou, C.W., Alexseyev, L., Kong, J., Dai, H.J., 2000. Controllable reversibility of an sp(2) to sp(3) transition of a single wall nanotube under the manipulation of an AFM tip: a nanoscale electromechanical switch?. Phys. Rev. Lett. 84 (21), 4950–4953.

Liu, L., Jayanthi, C.S., Wu, S.Y., 2001a. Structural and electronic properties of a carbon nanotorus: effects of delocalized and localized deformations. Phys. Rev. B 64(3), art. no. 033412.

Liu, B.B., Sundqvist, B., Andersson, O., Wagberg, T., Nyeanchi, E.B., Zhu, X.M., Zou, G.T., 2001b. Electric resistance of single-walled carbon nanotubes under hydrostatic pressure. Solid State Commun. 118 (1), 31–36.

Maiti, A., 2000. Mechanical deformation in carbon nanotubes—bent tubes vs tubes pushed by atomically sharp tips. Chem. Phys. Lett. 331 (1), 21–25.

Mazzoni, M.S.C., Chacham, H., 2000a. Atomic restructuring and localized electron states in a bent carbon nanotube: a first-principles study. Phys. Rev. B 61 (11), 7312–7315.

Mazzoni, M.S.C., Chacham, H., 2000b. Bandgap closure of a flattened semiconductor carbon nanotube: a first-principles study. Appl. Phys. Lett. 76 (12), 1561–1563.

Milstein, F., 1980. Review: theoretical elastic behaviour at large strains. J. Mater. Sci. 15, 1071–1084.

Nardelli, M.B., 1999. Electronic transport in extended systems: application to carbon nanotubes. Phys. Rev. B 60 (11), 7828–7833.

Nardelli, M.B., Bernholc, J., 1999. Mechanical deformations and coherent transport in carbon nanotubes. Phys. Rev. B 60 (24), R16338–R16341.

Nardelli, M.B., Fattebert, J.L., Orlikowski, D., Roland, C., Zhao, Q., Bernholc, J., 2000. Mechanical properties, defects and electronic behavior of carbon nanotubes. Carbon 38 (11–12), 1703–1711.

Paulson, S., Falvo, M.R., Snider, N., Helser, A., Hudson, T., Seeger, A., Taylor, R.M., Superfine, R., Washburn, S., 1999. In situ resistance measurements of strained carbon nanotubes. Appl. Phys. Lett. 75 (19), 2936–2938.

Peng, S., Cho, K., 2002. Nano electro mechanics of semiconducting carbon nanotube. J. Appl. Mech.-Trans. ASME 69 (4), 451–453.

Rochefort, A., Avouris, P., Lesage, F., Salahub, D.R., 1999. Electrical and mechanical properties of distorted carbon nanotubes. Phys. Rev. B 60 (19), 13824–13830.

Rosenblatt, S., Yaish, Y., Park, J., Gore, J., Sazonova, V., McEuen, P.L., 2002. High performance electrolyte gated carbon nanotube transistors. Nano Lett. 2 (8), 869–872.

Saito, R., Dresselhaus, G., Dresselhaus, M.S., 1998. Physical Properties of Carbon Nanotubes. Imperial College Press, London.

Tadmor, E.B., Smith, G.S., Bernstein, N., Kaxiras, E., 1999. Mixed finite element and atomistic formulation for complex crystals. Phys. Rev. B 59, 235–245.

Tombler, T.W., Zhou, C.W., Alexseyev, L., Kong, J., Dai, H.J., Liu, L., Jayanthi, C.S., Tang, M.J., Wu, S.Y., 2000. Reversible electromechanical characteristics of carbon nanotubes under local-probe manipulation. Nature 405 (6788), 769–772.

Weiner, J.H., 1983. Statistical Mechanics of Elasticity. Wiley, New York.

Xu, C.H., Wang, C.Z., Chan, C.T., Ho, K.M., 1992. A transferable tight-binding potential for carbon. J. Phys.: Condens. Matter 4, 6047–6054.

Yang, L., Anantram, M.P., Han, J., Lu, J.P., 1999. Band-gap change of carbon nanotubes: effect of small uniaxial and torsional strain. Phys. Rev. B 60 (19), 13874–13878.

Zhang, P., Huang, Y., Geubelle, P.H., Hwang, K.C., 2002a. On the continuum modeling of carbon nanotubes. Acta Mech. Sinica 18 (5), 528–536.

Zhang, P., Huang, Y., Geubelle, P.H., Klein, P.A., Hwang, K.C., 2002b. The elastic modulus of single-wall carbon nanotubes: a continuum analysis incorporating interatomic potentials. Int. J. Solids Struct. 39, 3893–3906.